17th AIAA/CEAS Aeroacoustics Conference (32nd AIAA Aeroacoustics Conference)
05 - 08 June 2011, Portland, Oregon

AIAA 2011-2747

Investigation of high supersonic jet noise: non-linear propagation effects and flow-acoustics correlations

Nicolas de Cacqueray* , **Christophe Bogey†** and **Christophe Bailly‡**

Laboratoire de Mécanique des Fluides et d'Acoustique

UMR CNRS 5509, Ecole Centrale de Lyon

69134 Ecully, France

In this paper, the data obtained by LES for an initially laminar and overexpanded jet at Mach number 3.3 and Reynolds number 10^5 are reexamined in order to investigate the non-linear effects on the propagation of the acoustic waves, and the normalized flow/acoustics cross-correlations. To study the non-linear propagation effects at the direction $\phi = 60^\circ$ and up to 240 radii from the nozzle exit, the LES near field is propagated in far-field by solving either the isentropic linearized Euler equations or the full Euler equations. The comparisons of the acoustic data obtained from the two methods clearly show that the non-linear effects are strong up to about 240 radii from the nozzle exit. Using the far-field acoustic results from the non-linear propagation, the normalized cross-correlations between the turbulent flow quantities and the acoustic pressure signals at the direction $\phi = 60^\circ$ are then evaluated to give some information on sound generation. A sound source which may be similar to that one observed in subsonic jets is first found on the jet axis in the vicinity of the end of the potential core. Other sound sources attributed to the supersonic convection of turbulent vortices are noticed. Finally, the normalized cross-correlations between the fluctuating density along the jet axis and the acoustic pressure display correlation bands between the 3rd and the 5th shock cells. These bands might be linked with the screech generation mechanism.

I. Introduction

The acoustic field generated by supersonic jets contains multiple noise components,[1] such as turbulent mixing noise, Mach waves, broadband shock-associated noise, and screech tones. Some of these components radiate in the same direction,[2,3] which may lead to difficulties to quantify their relative contributions to the acoustic far field. The increase of computational ressources as well as the development of highly accurate methods[4–6] have fortunately permitted to solve the compressible and unsteady Navier-Stokes equations to compute directly the aerodynamic field and the acoustic field radiated by turbulent flows.[7–10] Such simulations have been successfully used to investigate sound mechanisms occuring in subsonic[11] and supersonic[9,10] jets, as well as their sensivities to the nozzle-exit conditions.[12,13]

In a previous work by the authors,[10] an overexpanded supersonic jet at an exit Mach number of $M_e = 3.3$, an exit temperature of $T_e = 360$K and an exit static pressure of $p_e = 0.5 \times 10^5$ Pa has been computed by large-eddy simulation (LES). The jet is initially laminar, and originates from a straight pipe nozzle of radius r_e with a $0.05 r_e$ wide lip. The Reynolds number based on the nozzle-exit conditions is Re $\simeq 10^5$. The turbulent flow field as well as the acoustic near field have been investigated using azimuthal decompositions. The acoustic field propagated to a distance of 80 radii from the nozzle exit by solving the Euler equations has been studied in the same way. Contributions of Mach waves, turbulent mixing noise, broadband shock-assiociated noise, and screech noise have been identified by showing connections between the turbulent flow field and the acoustic fields.

*Phd student, nicolas.cacqueray@ec-lyon.fr

†CNRS Research Scientist, AIAA Member, christophe.bogey@ec-lyon.fr

‡Professor at Ecole Centrale de Lyon & Institut Universitaire de France, Senior AIAA Member, christophe.bailly@ec-lyon.fr

In the present paper, the data obtained for this jet are reexamined. The non-linear effects on the propagation of the acoustic waves are first investigated at $\phi = 60°$. Indeed, Gee *et al.*[14] and Saxena *et al.*[15] have shown that these effects can be important for supersonic jets. In order to study the non-linear propagation effects, two far-fied wave extrapolations are performed from the LES near field up to 240 radii from the nozzle exit. The first extrapolation is realized by solving the isentropic linearized Euler equations, whereas the second one is done by solving the full Euler equations. The contributions of the non-linear effects at $\phi = 60°$ are thus estimated by comparing the results from these two calculation in both time and frequency domains. Using the data from the non-linear propagation, the normalized cross-correlations between the acoustic pressure and the fluctuating axial velocity u'_z, the normal stress in the radial direction u'^2_r, the norm of the vorticity $|\omega|$ and the fluctuating density ρ' along the jet centerline and the shear layer are then evaluated. Cross-correlations between flow and acoustic fields have indeed been successfully used to provide information on noise generation mechanisms occurring in subsonic and supersonic jets.[3,11,16,17] In the present work, the time delay of the correlation spots are in particular investigated by using the acoustic propagation time and time delays estimated from flow characteristics such as the convection velocity. Results are also compared to a previous analysis of flow/acoustics correlations in subsonic jets.[11]

The paper is organized as follows. The jet exit conditions as well as the numerical parameters are first given in section II. The non-linear propagation effects of the acoustic waves in the downstream direction are then studied in section III. Normalized cross-correlations calculated between the turbulent flow and acoustic fields are presented in section IV. Finally, concluding remarks are given in section V.

II. LES computation

A. Jet parameters

An overexpanded jet at an exit Mach number of $M_e = 3.30$, an exit temperature of $T_e = 360$ K and an exit static pressure of $p_e = 0.5 \times 10^5$ Pa, is considered. The stagnation pressure and temperature are 28.6×10^5 Pa and 1144 K. The specific heat ratio is constant, and equal to 1.4, and the resulting exit velocity is $u_e = 1255$ m.s^{-1}. The flow originates at $z = 0$ from a straight pipe nozzle of radius $r_e = 1.6$ mm, with $0.05r_e$ wide lip, and of length $0.5r_e$. Inside the pipe, a Blasius profile for a laminar boundary layer of thickness $\delta = 0.05r_e$ is imposed for the mean velocity, and a Crocco-Busemann profile is used for the mean density. Random pressure disturbances of low amplitude are introduced in the nozzle, yielding nozzle-exit maximum velocity fluctuations of 1% of the jet exit velocity. The Reynolds number estimated from the exit quantities is equal to $Re = 2r_e u_e \rho_e/\mu_e = 0.94 \times 10^5$, where ρ_e and μ_e are the jet exit density and molecular viscosity. The equivalent fully-expanded exit conditions defined from the same stagnation conditions and a static pressure of $p_j = 10^5$ Pa are a Mach number of 2.83, a temperature of 439 K and a radius of $r_j = 0.81r_e$. The acoustic Mach number M_a, defined as the ratio of the fully-expanded velocity $u_j = 1190$ m.s^{-1} over the ambient sound speed $c_{amb} = 343$ m.s^{-1} is 3.47.

The simulation has been performed by solving the unsteady compressible Navier-Stokes equations in cylindrical coordinates, using low-dispersion and low-dissipation finite-difference schemes:[5,6,18] explicit 11-point 4th-order finite differences and 6th-order filter for space discretization, and a 2th-order 6-stage Runge-Kutta algorithm for time integration. For the treatment of the axis singularity, the method proposed by Mohseni & Colonius[19] is used, and to increase the time step, the effective azimuthal resolution is reduced near the jet centerline.[20] The LES approach is based on the explicit application of a relaxation filtering to the flow variables[21] to take into account the dissipative effects of the subgrid scales. Non-reflective acoustic boundary conditions[22] are implemented at the radial and upstream boundaries, and a sponge zone is used in the downstream direction to minimize acoustic reflections at the outflow boundary.[22] An adaptative and conservative shock-capturing method is in addition used to remove Gibbs oscillations near shocks.[18] This procedure combines a shock sensor informed by the local flow dilatation and a 2nd-order optimized filter. The grid used contains $n_r \times n_\theta \times n_z = 256 \times 128 \times 840 = 28 \times 10^6$ points. The LES data are recorded on two surfaces. The first one is located at $z = 0$, from $r = 1.15r_e$ to $r = 9.5r_e$, and the second one is at $r = 9.5r_e$, from $z = 0$ to $z = 52r_e$.

Snapshots of the density gradient norm, of the azimuthal vorticity, and of the fluctuating pressure p' are shown in figure 1. Inside the jet, a shock-cell structure is clearly found, and the turbulent development of the flow can be observed. High-amplitude acoustic waves are travelling into the downstream direction. Upstream-propagating waves, associated with the broadband shock-associated noise and to the screech,[10] are also visible.

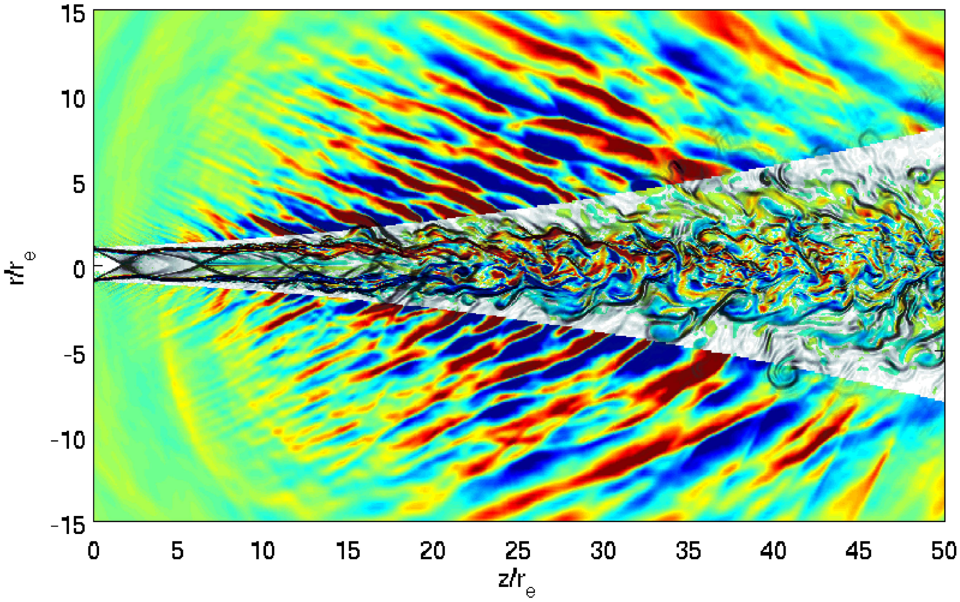

Figure 1. Snapshots in the (z, r) plane: density gradient norm and azimuthal vorticity in the jet, and fluctuating pressure p' outside the jet. The color scale ranges for levels from -5000 to 5000 Pa for p', and distances have been normalized by the nozzle radius r_e.

B. Description of the jet flow field

The main features of the jet flow fields are now provided. A more detailed description is available in de Cacqueray *et al.*[10] The properties of the mean jet flow field on the jet axis are first represented in figure 2. The centerline variations of the mean static pressure $< p >$ are shown in figure 2(a) using a scaling with the ambient static pressure p_{amb}. Six shock cells resulting from the adjustement of the jet exit static pressure p_e to the ambient pressure p_{amb} are observed. The amplitude of the pressure oscillations is found to decrease with the axial position. The evolution of the inverse of the mean centerline velocity u_{axis} normalized by the exit velocity u_e is displayed in figure 2(b). The mean axial velocity is modulated by the shock-cell structure. The ends of the potential core and of the sonic core, estimated here with the two criteria $u_{axis} = 0.9u_e$ and $u_{axis} = c$, where c is the local speed of sound, are respectively located at $z = 20r_e$ and $z = 36r_e$ from the nozzle exit.

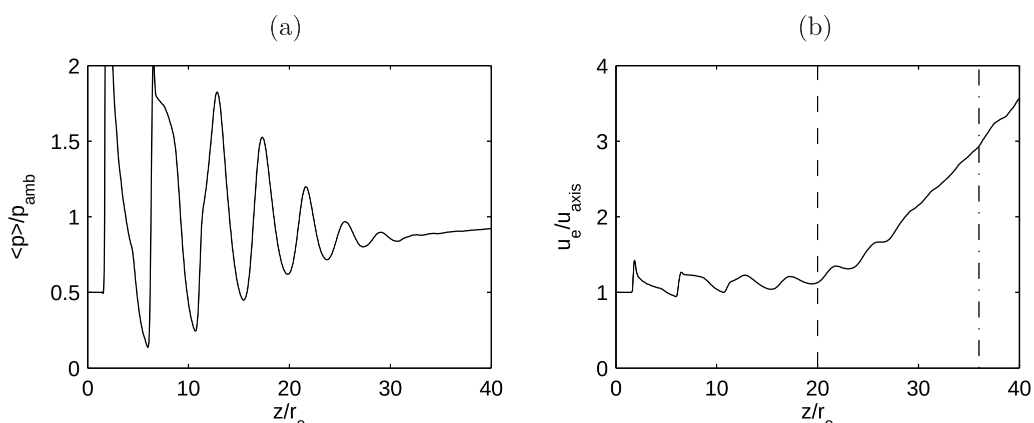

Figure 2. Variations of (a) the mean static pressure $< p >$ along the jet centerline, and (b) the inverse of the mean longitudinal velocity u_{axis}; $- - -$ end of the potential core $z_c = 20r_e$, and $- - -$ end of the sonic core $z_s = 36r_e$.

The variations of the rms values of the axial and radial velocities u'_z and u'_r, and of the density ρ' are presented in figure 3 along the jet axis and along the line $r = r_j$. Along the jet centerline in figure 3(a), the rms velocities increase slowly in the jet potential core. They reach their maxima at $z \simeq 25r_e$ which is downstream of the end of the potential core. The values of ρ_{rms} also increase in the jet potenial core, but they appear more disturbed by the shock-cell structure, in particular between $z = 10$ and $27r_e$. Along the shear layer in figure 3(b), the maximum of the rms values of the velocity u'_z is noticed upstream the end of the jet potential core, located here at $z_c = 20r_e$, whereas the maxima of the rms values of u'_r and ρ' are reached farther downstream, around $z \simeq 25r_e$.

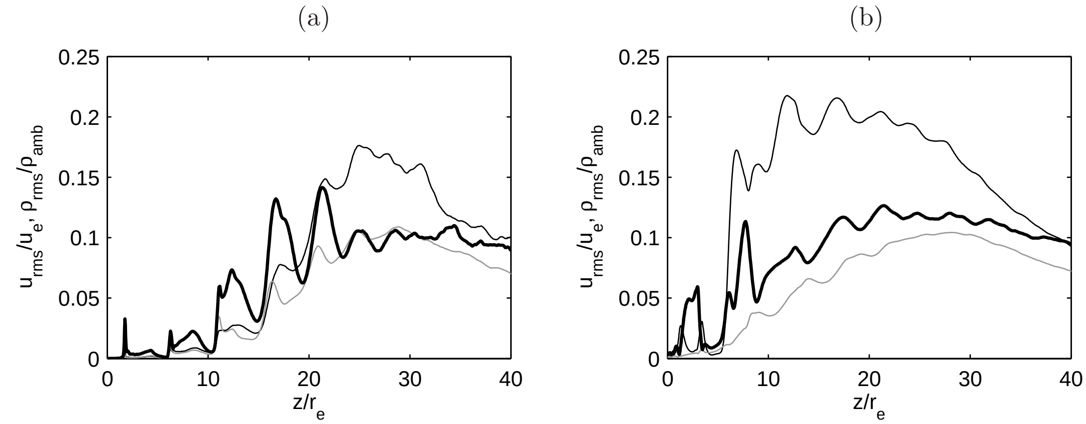

Figure 3. Variations of the rms quantities of —— u'_z, —— u'_r, and —— ρ' along (a) the jet axis, and (b) the line $r = r_j$.

The convection velocity u_c of turbulent vortices along the jet shear layer is presented in figure 4(a). The convection velocity is obtained from cross-correlations of the axial velocity fluctuations u'_z along the line $r = r_j$, and it is scaled by the jet exit velocity u_e. Near the nozzle, u_c is strongly modulated by the shock-cell structure and its estimation may not fully accurate. The existence of a mean convection velocity could also be questionnable in this region. It is possible to noticed that the convection velocity decreases downstream of $z \simeq 25r_e$. The sonic line $u_c = c_{amb}$ is also reported in figure 4(a). For $z > 5r_e$, the convection velocity estimated along the line $r = r_j$ is supersonic compared to the ambient sound speed. Consequently, Mach waves are expected to be generated in the present jet.

The convection velocity along the shear layer is now compared in figure 4(b) with that obtained along the jet centerline. Downstream of $z = 17r_e$, the convection velocity estimated along the jet axis is higher: the value of u_c along the line $r = 0$ increases from $z = 17$ to $19.5r_e$, and decreases downstream of the latter position. The peak value is thus reached near the end of the potential core at $z = 19.5r_e$, and it is equal to 75% of the jet exit velocity.

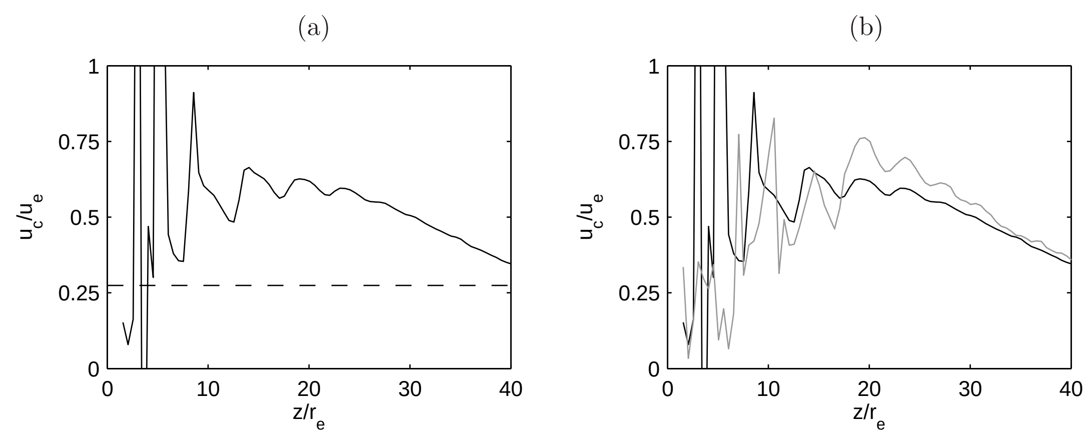

Figure 4. Variations of the convection velocity u_c estimated by cross-correlations of the axial velocity fluctuations u'_z; (a) —— u_c at $r = r_j$ and – – – line indicating $u_c = c_{amb}$; (b) —— u_c at $r = r_j$ and —— u_c along the jet axis.

III. Study of the non-linear propagation effects

A. Far-field wave extrapolations

To investigate the non-linear effects of the propagation of the acoustic waves, two far-field wave extrapolations from the LES data obtained on control surfaces at $z = 0$ and $r = 9.5r_e$ are carried out, one by solving the isentropic linearized Euler acoustic equations (ILEE), another by solving the full Euler equations. The same numerical methods as in the LES are employed except for a 4-th order filter used for the shock-capturing procedure because weak shocks in that case. These computations are performed on a grid containing $n_r \times n_\theta \times n_z = 2250 \times 64 \times 1950 = 280 \times 10^6$ points, with a grid size of $\Delta r = \Delta z = 0.1r_e$.

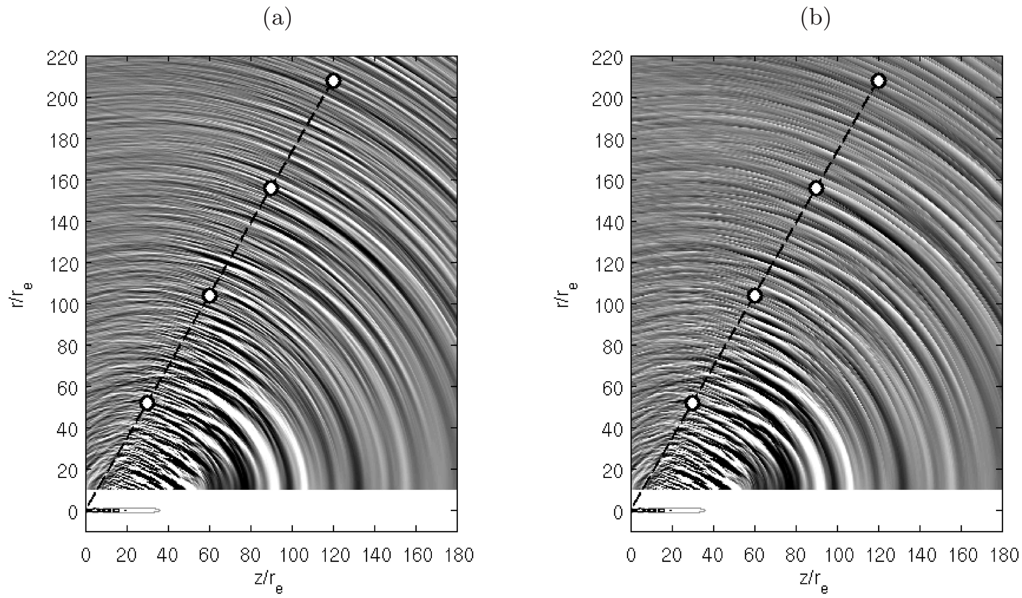

Figure 5. Snapshots of the fluctuating pressure obtained from (a) the linear and (b) the non-linear far-field wave extrapolations; the grey scale ranges from -600 Pa to 600 Pa. Inside the jet: —— $< u_z > /u_e = 0.9$ and —— $< u_z > /c = 1$; outside the jet: – – – radiation angle $\phi = 60°$ and ○ distance $d = 60r_e$, $120r_e$, $180r_e$ and $240r_e$ from the nozzle exit.

Snapshots of pressure obtained from the linear and the non-linear far-field wave extrapolations are provided at the same time in figures 5(a) and 5(b). The pressure waves propagate mainly in the downstream direction, and their levels seem higher for the linear propagation in figure 5(a). The propagation direction corresponding to an angle of $\phi = 60°$ relative to the jet flow direction at the nozzle exit is represented by a dashed line in the same figures. Along this line, the distances of $d = 60$, 120, 180 and $240r_e$ from the nozzle exit are represented by white circles. To finally give a first glimpse into the origin of the acoustic waves origin in the jet, the contour lines corresponding to mean axial velocities $< u_z >= 0.9u_e$, and $< u_z >= c$, where c is the local sound speed, have been depicted inside of the jet flow. Their intersection with the jet axis is used here to estimate the ends of the potential and of the sonic core, respectively located at $z_c = 20r_e$ and $z_s = 36r_e$ from the nozzle exit.

The noise levels at $240r_e$ from the nozzle exit are provided for both propagations in figure 6 as a function of the directivity angle ϕ. They are computed by integrating the pressure spectra from Strouhal number $St_e = 2fr_e/u_e = 0.023$ to 1, where f is the frequency. The noise levels obtained from the linear propagation exhibit a distinct peak at $\phi = 60°$. Those calculated from the full Euler equations are lower, and the peak at $\phi = 60°$ is less marked. At this angle, the difference of noise levels is around 5dB. Non-linear propagation effects of the acoustic waves thus play an important role for the present jet.

B. Investigation of the non-linear propagation effects

Non-linear propagation effects are now studied by comparing results from the linear and non-linear wave extrapolations along the direction $\phi = 60°$. The time signals of the acoustic pressure obtained at $\phi = 60°$ at distances $d = 60$, 120, 180, and $240r_e$ from the nozzle are first presented in figure 7. The time t is normalized

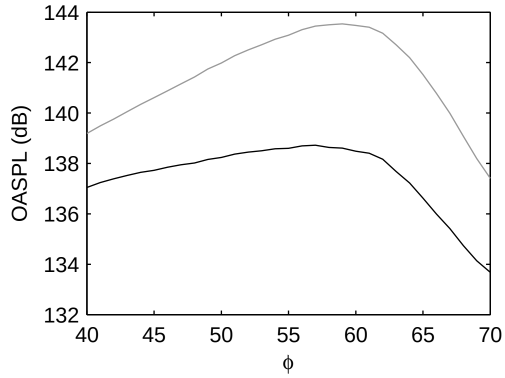

Figure 6. Overall sound pressure levels at $d = 240r_e$ from: —— the non-linear wave extrapolation, —— the linear wave extrapolation

by $u_e/2r_e$, and is delayed by $\tau = d/c_{amb}$. At $60r_e$ from the nozzle in figure 7(a), the shape and the levels of the pressure signals obtained using the two extrapolation methods are close. However, some discrepancies due to the non-linear effects can be observed, at the time $t - \tau \simeq 190$ for instance. When the distance from the nozzle exit increases, the amplitude of the acoustic waves computed with the full Euler equations becomes lower than those calcuted using the linear acoustic equations. Moreover, weak shock waves gradually appear on the acoustic signal obtained from the non-linear propagation. At $240r_e$ from the nozzle in figure 7(d), the pressure signal finally looks as a sequence of N-waves.

(a) (b)

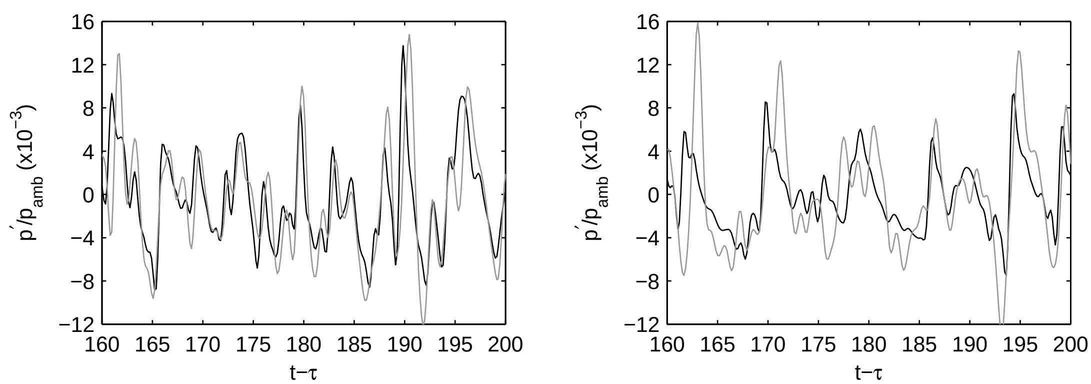

(a) (b)

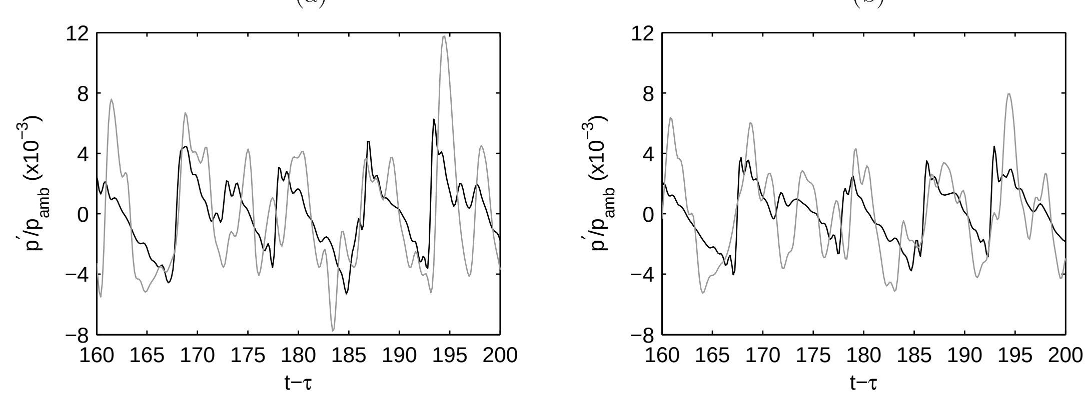

Figure 7. Pressure signals at $\phi = 60°$ and (a) $d = 60r_e$, (b) $120r_e$, (c) $180r_e$, and (d) $240r_e$ from the nozzle exit from: —— the non-linear wave extrapolation, —— the linear wave extrapolation

As expected, the non-linear propagation effects distord the acoustic signal. These effects are now investigated in the frequency domain in figure 8. In this figure, the spectra corresponding to the time signals shown previously in figure 7 are presented as a function of the Strouhal number St_e. At $d = 60r_e$ from the nozzle exit, spectra from the linear and the non-linear propagations are found to differ appreciably for $St_e > 0.1$. The noise levels computed using the Euler equations are lower than those obtained from the linear acoustic equations for $0.1 < St_e < 0.9$, and they are higher for $St_e > 0.9$. When the distance from the nozzle increases, the non-linear effects seem to accumulate. The maximum of the spectrum for the non-linear propagation decreases compared to that from the linear propagation, and its frequency moves toward lower Strouhal numbers. Furthermore, the contributions of high frequencies increase due to non-linear effects. At $240r_e$ from the nozzle, a rise is indeed clearly observed for $St_e > 0.8$. According to Saxena *et al.*,[15] this trend is typical of non-linear propagation effects.

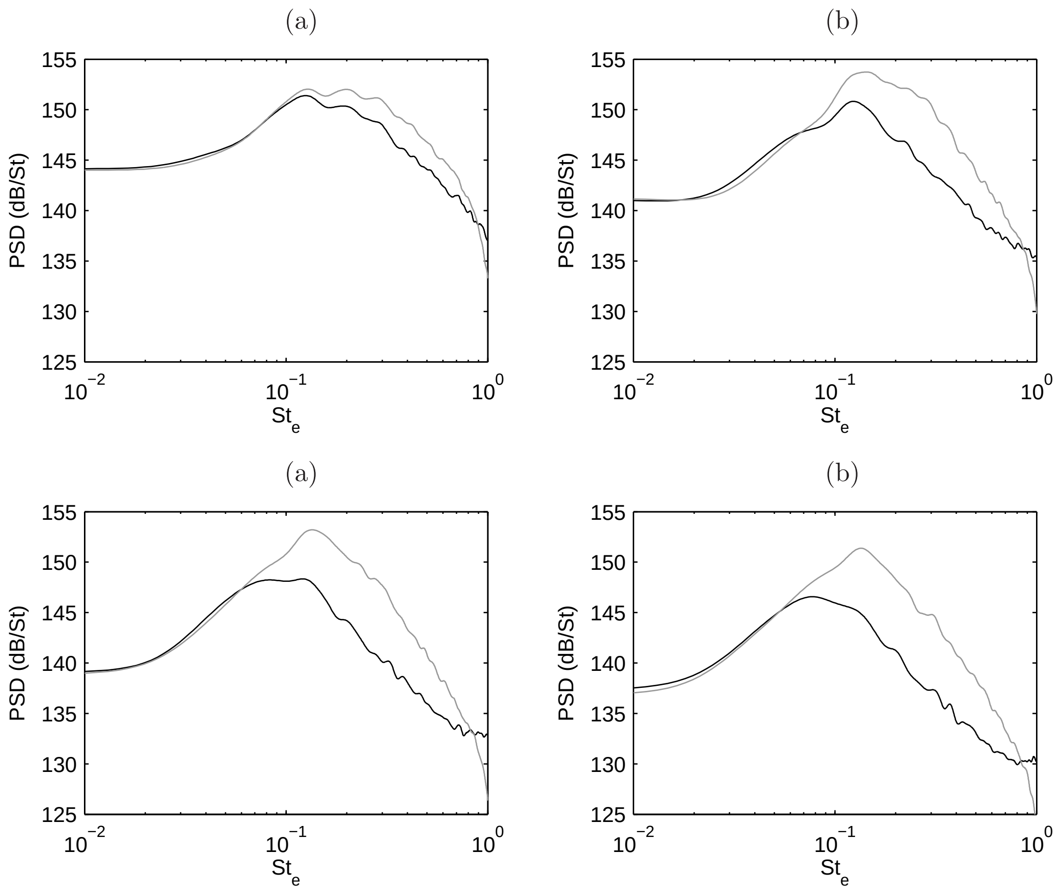

Figure 8. Acoustic spectra at $\phi = 60°$ and at (a) $d = 60r_e$, (b) $120r_e$, (c) $180r_e$, and (d) $240r_e$ from the nozzle exit from: ——— the non-linear wave extrapolation, and ——— the linear wave extrapolation

Along the line $\phi = 60°$, the non-linear propagation effects are now studied more quantitatively. The differences between spectra obtained for the non-linear propagation and for the linear propagation are displayed in figure 9 at distances $d = 60r_e$, $120r_e$, $180r_e$ and $240r_e$ from the nozzle. At these four distances, up to $St_e \simeq 0.06$, no appreciably discrepancy is noticed between the linear and the non-linear wave extrapolations. For $0.06 < St_e < 0.85$, the differences between the results are negative, which indicating that the noise components here contain lower energy because of the non-linear propagation effects. In this range of Strouhal numbers, the peak discrepancy increases with the distance from the nozzle exit, and moves toward lower frequencies. At $d = 240r_e$, it reaches -7.8 dB at $St_e \simeq 0.23$ for instance. For $St_e > 0.85$, the differences between the spectra become positive. Therefore, these components are enhanced, and certainly receive energies from the lower frequencies. It is finally interesting to note that the differences observed at $d = 180r_e$ and $d = 240r_e$ are close. Consequently, the non-linear effects may be rather weak at large distances from the nozzle exit.

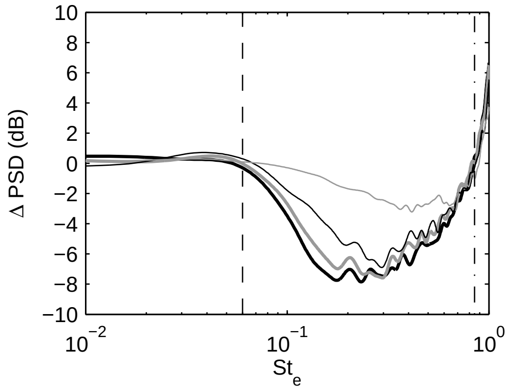

Figure 9. Differences between the power spectral densities obtained for the non-linear and linear wave extrapolations at $\phi = 60°$ and —— $d = 60r_e$, —— $120r_e$, —— $180r_e$, and —— $240r_e$ from the nozzle exit; − − − $St_e = 0.06$, and − · − · $St_e = 0.85$.

IV. Flow-acoustics correlations

The sound sources radiating in the downstream direction are investigated using normalized cross-correlations between the turbulent flow and acoustic fields obtained for the present jet. For this purpose, the turbulent quantities u'_z, $u'_r u'_r$, $|\omega|$ and ρ', which are respectively the fluctuating axial velocity, the normal stress in the radial direction, the norm of the vorticity and the fluctuating density, are recorded in the jet along the centerline and along the line at $r = r_j$. The fluctuating acoustic pressure p', obtained from the non-linear wave extrapolation, is collected at $\phi = 60°$, at distances $d = 60r_e$, $120r_e$, $180r_e$ and $240r_e$ from the nozzle exit. These locations are represented by white circles in figure 5(b). The normalized correlations between u'_z, $u'_r u'_r$, $|\omega|$ and ρ' at point $\mathbf{x}_1$ in the jet and the acoustic far-field pressure are calculated in the following way:

$$Cu_z p(\mathbf{x}_1, d, \tau) = \frac{< u'_z(\mathbf{x}_1, t) p'(d, t+\tau) >}{< u'^2_z(\mathbf{x}_1, t) >^{1/2} < p'^2(d, t) >^{1/2}}$$

$$Cu_r^2 p(\mathbf{x}_1, d, \tau) = \frac{< (u'^2_r(\mathbf{x}_1, t) - < u'^2_r(\mathbf{x}_1, t) >) p'(d, t+\tau) >}{< (u'^2_r(\mathbf{x}_1, t) - < u'^2_r(\mathbf{x}_1, t) >)^2 >^{1/2} < p'^2(d, t) >^{1/2}}$$

$$C|\omega| p(\mathbf{x}_1, d, \tau) = \frac{< |\omega|(\mathbf{x}_1, t) p'(d, t+\tau) >}{< |\omega|^2(\mathbf{x}_1, t) >^{1/2} < p'^2(d, t) >^{1/2}}$$

$$C\rho p(\mathbf{x}_1, d, \tau) = \frac{< \rho'(\mathbf{x}_1, t) p'(d, t+\tau) >}{< \rho'^2(\mathbf{x}_1, t) >^{1/2} < p'^2(d, t) >^{1/2}}$$

where $< \bullet >$ denotes time averaging, and τ is the time delay between the flow quantities and the far-field acoustic pressure. The position $\mathbf{x}_1$ is respectively equal to $(0, z)$ along the jet axis, and to (r_j, z) along the shear layer. Note finally that the normalized cross-correlations are averaged in the azimuthal direction.

A. Flow-acoustics correlations along the jet axis

The correlations between the flow quantities along the jet axis and the far-field acoustic pressure are first considered. The normalized cross-correlations between the turbulent signals u'_z, $u'_r u'_r$, $|\omega|$ and ρ', and the far-field pressure p' at $\phi = 60°$ and at $d = 60r_e$, $120r_e$, $180r_e$ and $240r_e$ from the nozzle exit are presented in figure 10 as funtions of the axial position along the jet axis z, and of the time delay τ normalized by $u_e/2r_e$. The locations of the ends of the potential core and of the sonic core, respectively at $z_c = 20r_e$ and $z_s = 36r_e$, are also indicated. The time delay corresponding to the linear propagation of an acoustic wave from the position where the turbulent quantity is recorded to the one where the far-field pressure is collected is also shown in the figure. This time delay is thus r_{acou}/c_{amb}, where r_{acou} is the distance between these two positions.

For the different turbulent quantities, the amplitude of the flow/acoustics correlations is low at $d = 60r_e$. It then increases with d, and significant levels are then observed for a time delay close to the acoustic

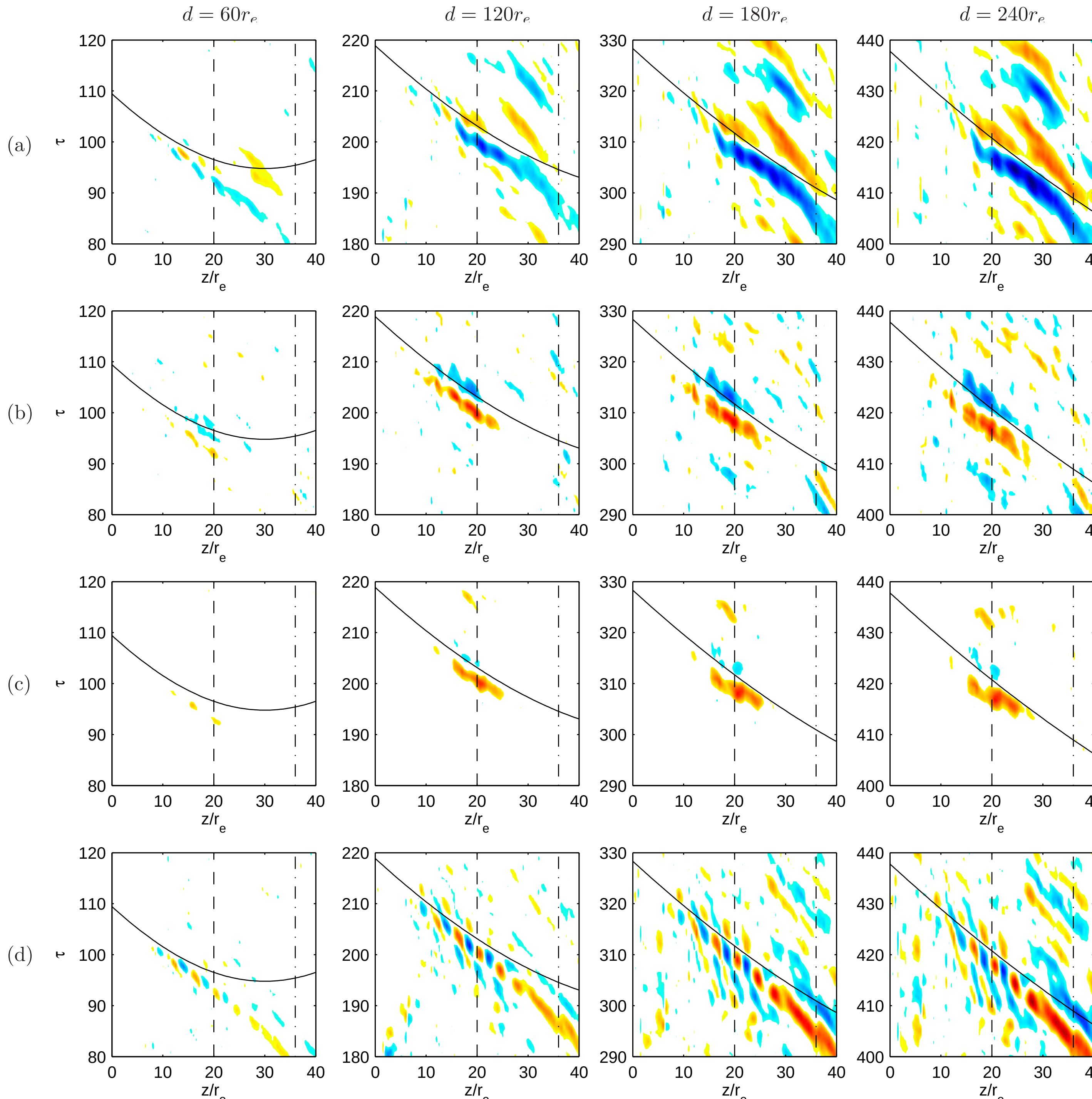

Figure 10. Normalized cross-correlations between the acoustic pressure p' at $\phi = 60°$ and at $d = 60r_e$, $120r_e$, $180r_e$ and $240r_e$ from the nozzleexit, and flow quantities along the jet centerline: (a) u'_z, (b) $u'_r u'_r$, (c) $|\omega|$, and (d) ρ' (X-axis: axial positions z/r_e along the jet centerline, Y-axis: time delay τ). ——— propagation time, — — — end of the potential core and — · — · end of the sonic core. Levels scale from -0.25 to 0.25 for (a) and (d), and from -0.15 to 0.15 for (b) and (c).

propagation time, which means that these correlation spots may be connected to noise generation. It can moreover be noticed that the correlation maps obtained for acoustic probes at $d = 180$ and $240r_e$ are close. Consequently, the geometrical convergence of the acoustic far field may be nearly reached at $d = 240r_e$.

The normalized cross-correlations between the flow variables and the acoustic signal collected at $d = 240$

are examined more in detail. The acoustic signal at this location is seen to strongly correlate with the axial velocity fluctuations downstream of the potential core in figure 10(a). Significant correlations are also observed for Cu_r^2p and $C|\omega|p$ in figures 10(b) and 10(c). They are however clustered around the end of the potential core at $z_c = 20r_e$. Finally in figure 10(d), the correlations between the fluctuating density along the jet axis and the acoustic signal at $\phi = 60°$ and $d = 240r_e$ are significant from $z = 12$ to $40r_e$. On the contrary to the other correlations, their sign varies in the axial direction. It is finally interesting to note that the correlation maps between u_z' and $|\omega|$ on the jet axis, and the acoustic signal in the downstream direction are similar to those obtained by Bogey & Bailly[11] and Bogey *et al.*[23] for subsonic round jets and hot coaxial jets respectively.

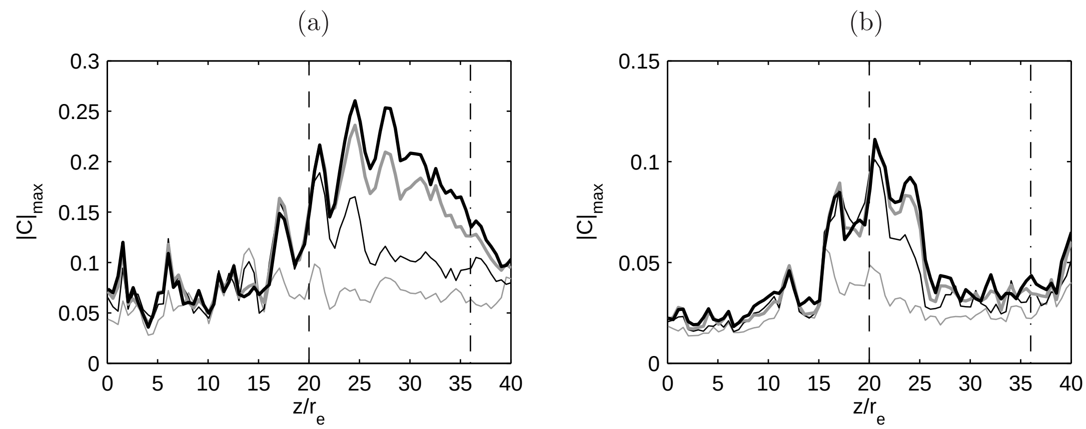

Figure 11. Variations of the peak value of the norm of the normalized cross-correlations beween the acoustic pressure p' at $\phi = 60°$ and $d = 60r_e$, $d = 120r_e$, $d = 180r_e$, and $d = 240r_e$ from the nozzle exit, and the turbulent quantities along the jet centerline: (a) u_z' and (b) $|\omega|$. end of the potential core and end of the sonic core.

More quantitative results are provided for Cu_zp and $C|\omega|p$. In figure 11, the axial variations of the maxima of the norm of these correlations are plotted for the acoustic propagation signal at $d = 60r_e$, $120r_e$, $180r_e$ and $240r_e$. In all cases, the axial evolution of the maxima displays oscillations which can be associated with the shock-cell structure in the jet plume. As it has been previously noted in figure 10(a), the norm of Cu_zp in figure 11(a) increases with d. The peaks of the normalized cross-correlations reach here 0.11, 0.19, 0.23 and 0.26 at $d = 60$, 120, 180 and $240r_e$ respectively. The axial location of these peaks furthermore moves from $z = 14r_e$ at $d = 60r_e$ to $z = 25r_e$ at $d = 240r_e$. Note that the latter position corresponds to the maximum of rms value of u_z' on the jet axis in figure 3(a). The peaks of the norm of $C|\omega|p$ also increase with d in figure 11(b), but they are limited to the vicinity of the potential core from $d = 120$ to $240r_e$. At $d = 240r_e$, the maximum value of $|C|\omega|p|$ is 0.11, and it is reached at $z = 20.5r_e$.

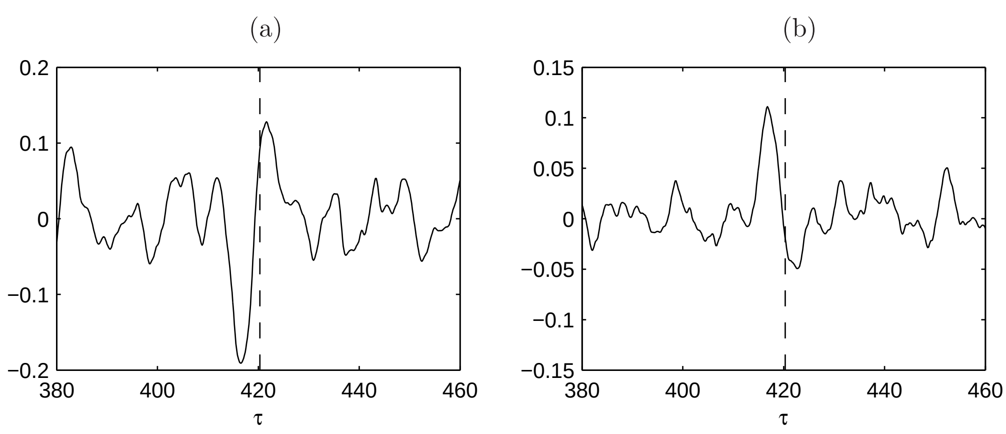

Figure 12. Normalized cross-correlations between (a) u_z' and (b) $|\omega|$ at $z = 20.5r_e$ on the jet axis, and the far-field pressure p' at $\phi = 60°$ and $d = 240r_e$. time delay for a linear acoustic wave.

The time signals of the normalized cross-correlations between u'_z and $|\omega|$ at $z = 20.5r_e$, and the far-field pressure p' at $\phi = 60°$ and $d = 240r_e$ are shown in figure 12. This axial position is just donwstream of the potential core located at $z_c = 20r_e$. The correlation peak is negative for Cu_zp and positive for $C|\omega|p$. In both cases, the time delay at the peak location is however slightly lower than the time estimated for a linear propagation.

The statistical properties of the flow quantities u_z and $|\omega|$ along the jet axis are now discussed. The axial variations of the skewness factor of u_z are first plotted in figure 13(a). A negative peak clearly emerges for $15r_e < z < 25r_e$ with a maximum value of -2.4 at $18.5r_e$. Consequently, strong deficits of velocity are likely to be found upstream of the end of the potential core.

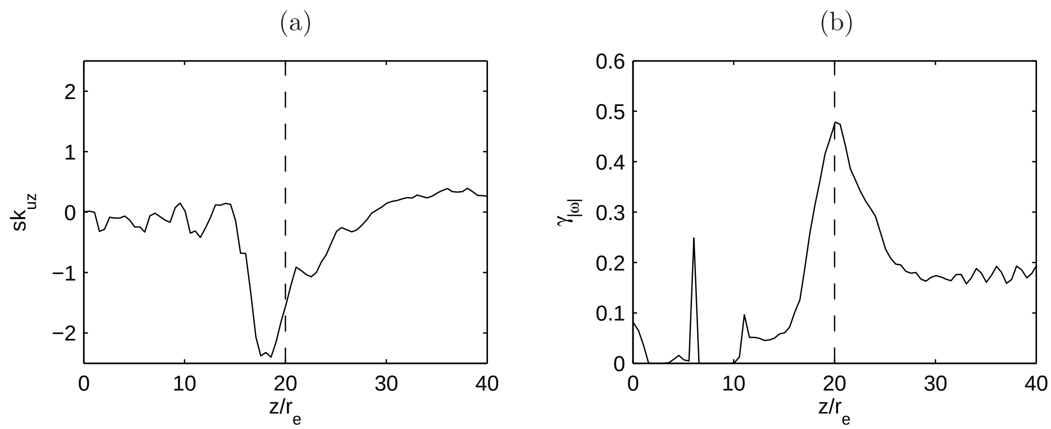

Figure 13. Variations of (a) the skewness factor of u_z and of (b) the intermittency factor calculated from the vorticity norm; — — — end of the potential core.

As it has been previously performed by Bogey & Bailly,[11] the intermittency of the centerline turbulence is then investigated. In a similar way, the function $I(t)$ defined by

$$I(t) = \begin{cases} 1 & \text{if } |\omega| \text{ is lower the } < |\omega| > /2, \\ 0 & \text{otherwise} \end{cases}$$

is computed. The intermittency factor $\gamma_{|\omega|}$ is obtained by averaging $I(t)$. One can thus expect $\gamma_{|\omega|} \simeq 0$ for a laminar vorticity signal, and $\gamma_{|\omega|} \simeq 1$ for an intermittent signal.[11] For the present jet, the axial variations of the intermittency factor are represented in figure 13(b). In the first part of the jet potential core, the intermittency factor is below 0.1, except at $z = 6r_e$ where a sharp peak is observed. The variations of $\gamma_{|\omega|}$ then display a noticeable increase near the end of potential core. A peak value of 0.47 is reached at $z = 20r_e$, which is also the axial location of the end of the jet potential core. Downstream of this position, the factor $\gamma_{|\omega|}$ decreases gradually down to final values close to 0.2. The signal of vorticity is therefore intermittent at the end of the jet potential core. A similar trend has been observed in subsonic jets by Bogey & Bailly,[11] and it has been associated with the intrusion of vortical structures into the jet core.

To look for possible explanations for the statistical results, time signals of $|\omega|$ and of $u_z - u_j$ at the end of the potential core are provided in the two top sub-plots of figure 14. The vorticity signal displays burst which may be associated with the intrusion of vortical structures into the jet core. Negative peaks of axial velocity occur intermittently at the same time as vorticity burst in the jet core. The velocity deficit can reach up to about 50% of u_j. The vorticity and the velocity time signals presented here are very similar to those observed in subsonic jets by Bogey & Bailly.[11] According to figure 4(b), the vortical structures introduced into the jet core may be accelerated near the end of the potential core at $z \simeq 20r_e$. In subsonic jets, this phenomenon may be assumed to be source of sound radiating in downstream direction.[11]

In the present jet, significant correlations for a time delay close to the acoustic propagation time have been found between the norm of the vorticity near $z = 20r_e$ and the acoustic pressure at $\phi = 60°$ in figure 10(c). The acoustic signal at $\phi = 60°$ and $d = 240r_e$ is thus shown in figure 14 for a time delay corresponding to its maximum of correlation with $|\omega|$ at $z = 20r_e$. Connections are noticed between the positive part of the acoustic signal and peaks of $|\omega|$ and u'_z which leads, as expected, to respectively positive and negative cross-correlations. Similar connections have also been observed in subsonic jets by Bogey &

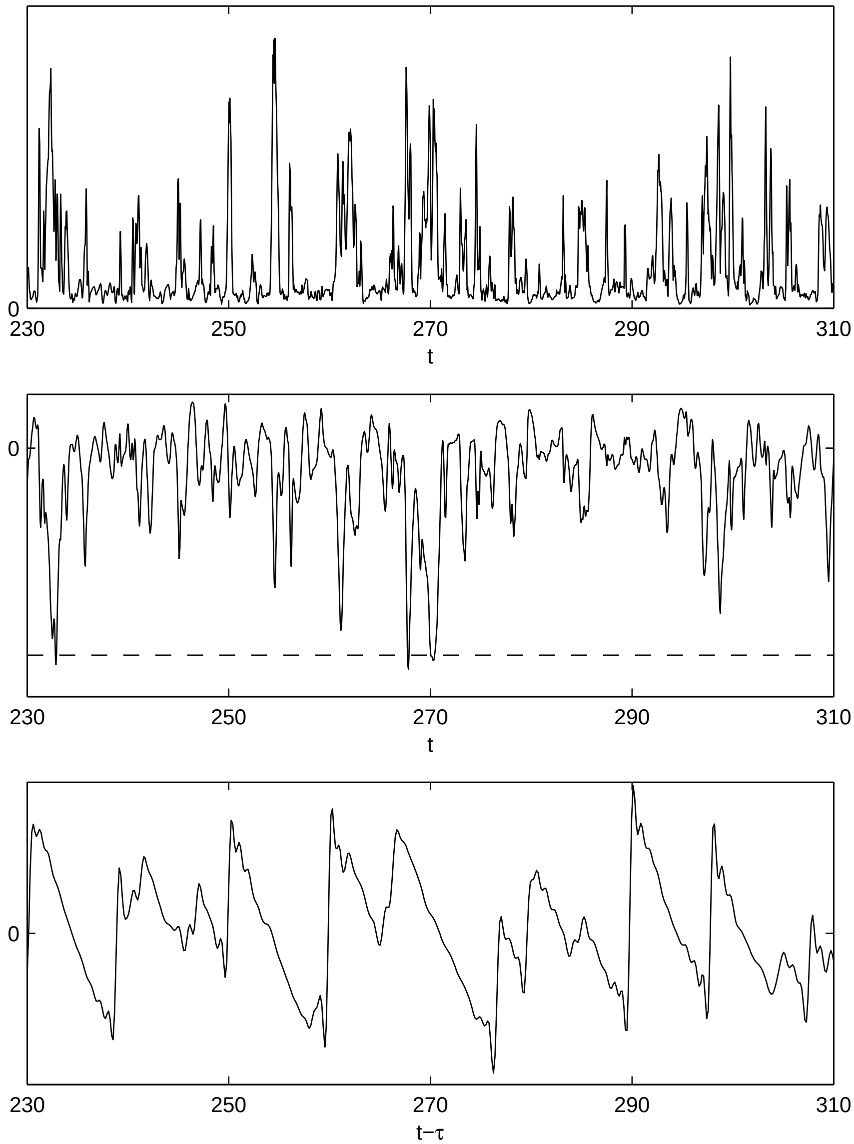

Figure 14. Time signal of (*top*) the norm of the vorticity $|\omega|$, and of (*middle*) the velocity $u_z - u_j$ at the end of the potential core on the jet axis, and of the acoustic pressure p' at $\phi = 60°$ and $d = 240r_e$ from the nozzle exit. The acoustic signal is delayed from the propagation time estimated using $C|\omega|p$ correlations. $---$ -50% of u_j.

Bailly.[11] Consequently, one could expect that the noise radiation mechanism observed at the end of the potential core by Bogey & Bailly[11] may occur in the present supersonic jet. This hypothesis is supported by the work of Tam *et al.*,[24] which have shown the continuity of the acoustic spectra in the downstream direction between subsonic and supersonic jets, suggesting same noise component in both cases.

B. Flow-acoustics correlations along the jet shear layer

The cross-correlations between the acoustic pressure at $\phi = 60°$, and the same turbulent quantities as previously are now evaluated along the jet shear layer. Correlation maps of Cu_zp, Cu_r^2p, $C|\omega|p$, and $C\rho p$ are presented in figure 15 as functions of the time delay τ and of the axial position z along the line $r = r_j$.

Regions with high levels of correlations are observed for a time delay corresponding to the acoustic propagation time. As it has been previouly remarked for cross-correlations along the jet axis, correlation maps at $d = 180r_e$ and at $d = 240r_e$ are very close, therefore the acoustic far field may be reached at $d = 240r_e$.

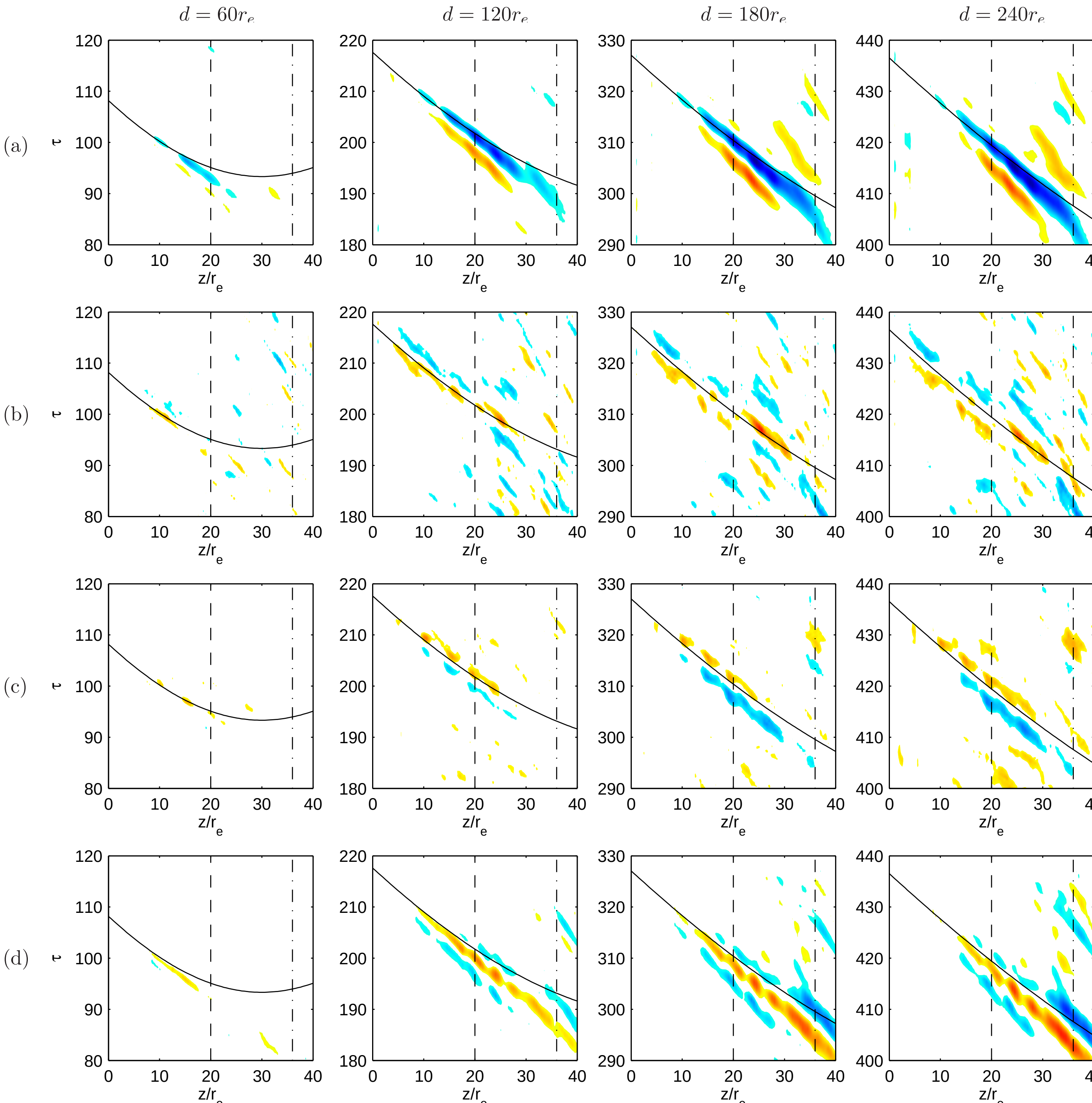

Figure 15. Normalized cross-correlations between the acoustic pressure p' at $\phi = 60°$ and $d = 60r_e$, $120r_e$, $180r_e$ and $240r_e$ from the nozzle exit, and flow quantities along the line $r = r_j$: (a) u'_z, (b) $u'_r u'_r$, (c) $|\omega|$, and (d) p' (X-axis: axial positions z/r_e along the line $r = r_j$, Y-axis: time delay τ). ——— propagation time, — — — end of the potential core and — · — · end of the sonic core. Levels scale from -0.25 to 0.25 for (a) and (d), from -0.10 to 0.10 for (b), and from -0.08 to 0.08 for (c).

At this distance and for a time delay close to acoustic propagation time, the axial velocity fluctuations display significant negative correlation coefficients with the acoustic pressure for $z = 12r_e$ to $36r_e$ in figure 15(a). The maximum of correlation is reached between the ends of the potential core and of the sonic core. Concerning the Cu_r^2p map in figure 15(b), appreciably correlation levels are observed for $z = 5r_e$

to $30r_e$. Noticeable correlation coefficients are also found for $C|\omega|p$ in figure 15(c) between $z = 12r_e$ and $z = 30r_e$. Following the acoustic propagation time, positive correlation coefficients between the fluctuating density and the acoustic pressure at $d = 240r_e$ are finally noted in figure 15(d).

Cross-correlation maps between the acoustic pressure at $d = 240r_e$ and turbulent quantities collected along the jet axis in figure 10, and the shear layer in figure 15 are compared. For Cu_zp maps in figures 10(a) and 15(a), the correlation coefficients have the same sign and nearly the same levels. Moreover their maxima are located downstream of the potential core in both maps. Upstream of the jet potential core, significant levels of correlations are however found following the trajectory of the acoustic propagation time along the jet shear layer in figure 15(a), which is not the case along the jet axis in figure 10(a). Larger discrepancies are observed for the other flow quantities. For instance, the amplitude of the cross-correlations are lower for $u_r'^2$ and $|\omega|$ along the shear layer than along the jet centerline. Furthermore, the $C\rho p$ coefficients exhibit sign variations along the jet axis in figure 10(d), which is not the case along the shear layer in figure 15(d).

The axial variations of the maximum of the norm of the Cu_zp and $C|\omega|p$ correlations are reported in figure 16 for acoustic probes at $d = 60r_e$, $120r_e$, $180r_e$ and $240r_e$ as a function of the position along the jet shear layer. In the figure 16(a), the levels of Cu_zp increase with the distance d. Their peak values reach 0.12, 0.19, 0.23, and 0.24 for $d = 60$, 120, 180 and $240r_e$, and they are located at $z = 15.5r_e$, $20r_e$, $24r_e$, and $24.5r_e$ respectively. The levels of these peaks as well as their axial positions fairly agree with the data found along the jet axis in figure 11(a). The maxima of $|C|\omega|p|$ shown in figure 16(b) do not vary much. Moreover, compared to the jet axis in figure 11(b), the levels of correlations are lower, and no distinct peak is noticed in the vicinity of the jet potential core at $z_c = 20r_e$.

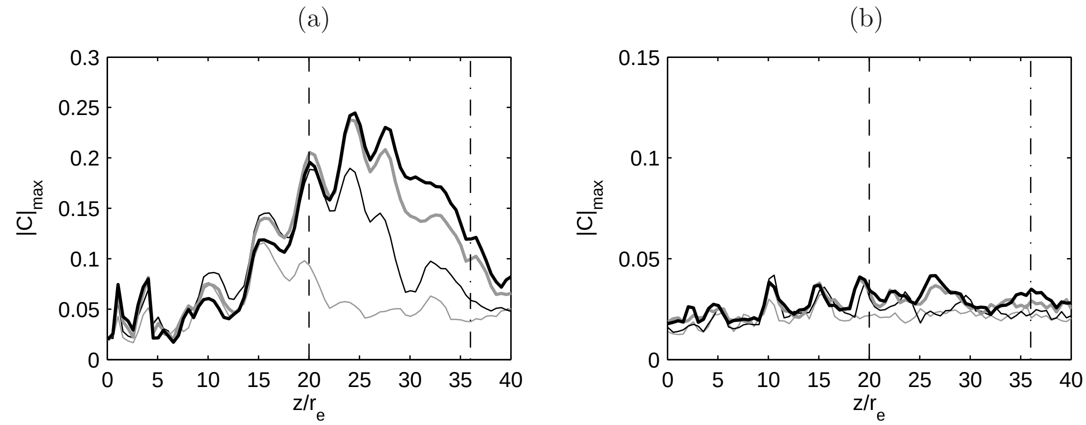

Figure 16. Maxima of normalized cross-correlations beween the acoustic pressure p' at $\phi = 60°$ and —— $60r_e$, —— $120r_e$, —— $180r_e$, and —— $240r_e$ from the nozzle, and turbulent quantities at $r = r_j$: (a) u_z' and (b) $|\omega|$. — — — end of the potential core and — · — · end of the sonic core.

The trajectory of the normalized cross-correlations between the fluctuation of axial velocity collected along the jet shear layer and the acoustic pressure at $\phi = 60°$ and $d = 240r_e$ is explored in figure 17. In the correlation map shown, the acoustic propagation time is also reported. As it has been previously noticed in figure 15(a), significant negative correlations are observed between $z = 12r_e$ to $z = 36r_e$. The corresponding time delay is found to agree very well with the acoustic propagation time for $z = 12r_e$ to $25r_e$. Downstream of this last position, the time delay is lower than the acoustic propagation time, and their difference increases with the axial position along the jet shear layer. Therefore, only the correlations between $z = 12r_e$ to $25r_e$ are related to noise generation.

The time delay τ_{conv} corresponding to the convection of the coherent structures[11] along the jet shear layer is also plotted in figure 17. This new time delay is based on the convection velocity u_c:

$$\tau_{conv}(z) = \tau_c(z_c) + \int_z^{z_c} \frac{dz}{u_c(z)}$$

where τ_c is the acoustic time delay esitmated at the point at $z_c = 20r_e$ and $r = r_j$, and u_c is the convection velocity along the jet shear layer provided in figure 4(a). The trajectory of the cross-correlations is found to follow the time delay based on the convection velocity in figure 17. Therefore, the significant levels of correlation observed downstream of $z = 25r_e$ may be associated with the convection of the noise sources.

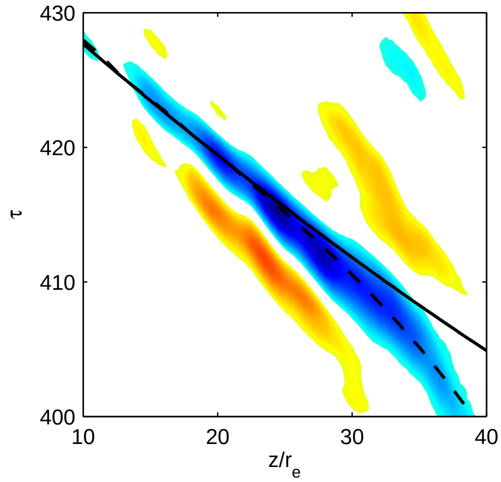

Figure 17. Normalized cross-correlations between the acoustic pressure at $d = 240r_e$ and the fluctuating axial velocity collected along the jet shear layer; ——— acoustic propagation time, and – – – time delay based on the convection velocity. Levels scale from -0.25 to 0.25

Finally, it can be noticed that between $z = 12r_e$ to $25r_e$ the time delay of the correlations agrees both with the acoustic propagation time and the time delay based on the convection of the coherent structures which here coincide. As the correlations vary in this region without sign change, one could expect that they are related to the same noise generation mechanism. According to this, the noise generation mechanism may be spread over a large axial extent, and related to the supersonic convection of turbulent structures. These trends fairly correspond to the description of the Mach wave mechanism given by Ffowcs Willams & Maidanik.[25]

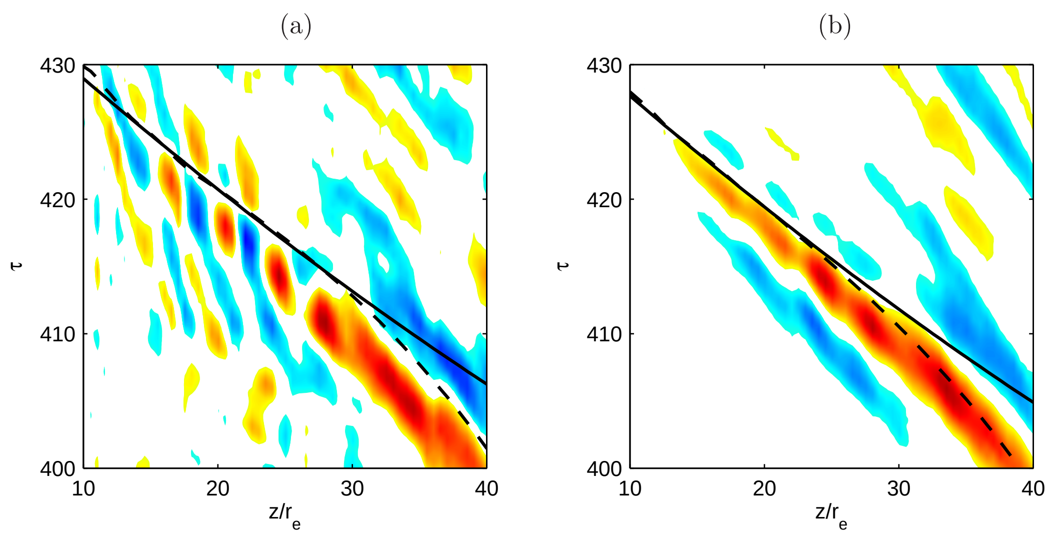

Figure 18. Normalized cross-correlations between the acoustic pressure and the fluctuating density along (a) the jet centerline, and (b) the shear layer; ——— acoustic propagation time r_{acou}/c_{amb}, and – – – time delay based on the convection velocity. The levels scale from -0.25 to 0.25

C. Investigation of the acoustic/ correlations

The correlations map between the pressure at $\phi = 60°$ and $d = 240r_e$ and the fluctuating densities collected along the jet axis and along the shear layer are finally compared in figure 18. In order to investigate the different correlation spots, the acoustic propagation time r_{acou}/c_{amb} is also reported in this figure. As it has been previously noticed in figures 10(d) and 15(d), significant correlation levels are found for a time

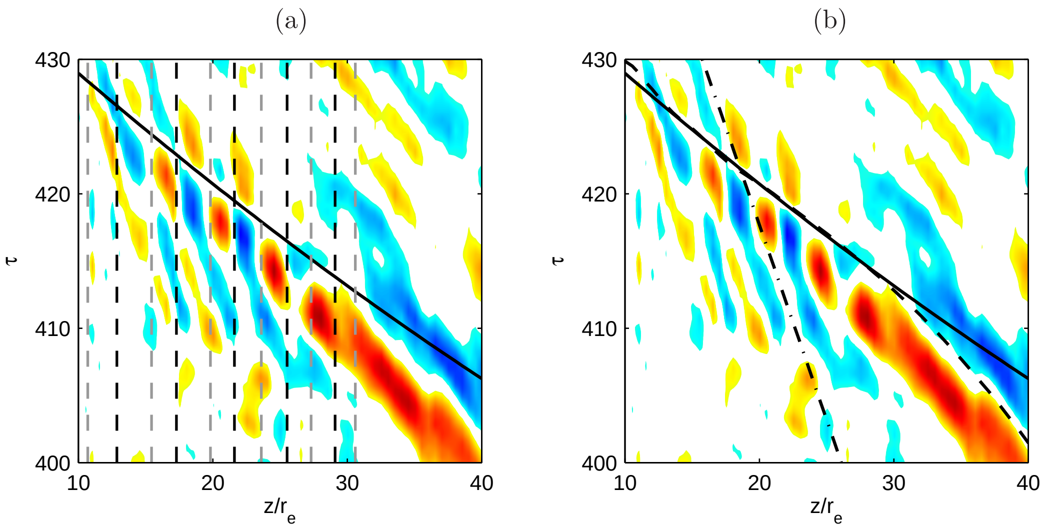

Figure 19. Normalized cross-correlations between the acoustic pressure and the fluctuating density along the jet axis. (a) ——— acoustic propagation time, — — — maxima of the mean static pressure on the jet axis, and — — — minima of the mean static pressure on the jet axis; (b) ——— acoustic propagation time, — — — time delay based on the convection velocity, and — · — · time delay based on the screech frequency. The levels scale from -0.25 to 0.25

delay close to the acoustic propagation time in figure 18. Following the acoustic propagation time, the sign of the correlation coefficients is found to vary periodically from $z = 12r_e$ to $25r_e$ along the jet centerline in figure 18(a), whereas it remains positive along the entire shear layer in figure 18(b). Along the jet axis in figure 18(a), successive bands of positive and negative correlations are indeed observed, crossing the acoustic propagation time. These intersections may thus be related to sound sources.

The time delay τ_{conv} associated with the convection of coherent structures is also displayed in figure 18. It is estimated from the convection velocity along the jet axis and the shear layer, and coincide at $z = 20r_e$ with the acoustic propagation time. The time τ_{conv} is found to collapse with the acoustic propagation time r_{acou}/c_{amb} from $z = 12r_e$ to $30r_e$ along the jet axis in figure 18(a) and from $z = 12$ to $25r_e$ along the shear layer in figure 18(b). Therefore, the time delay τ_{conv} cannot be useful to explain the successive bands of correlations observed in figure 18(a).

The bands of positive and negative correlations are now investigated in detail in figure 19. With this aim, the quasi-periodic variations of the correlation sign along the trajectory defined by the acoustic propagation time is studied in figure 19(a). As the jet is overexpanded, it appears natural to compare this periodic variations with the oscillations of the mean static pressure $< p >$ along the jet axis, shown previously in figure 2(a). Consequently, the maxima and the minima of $< p >$ have been reported in the $C\rho p$ correlation map in figure 19(a). The extrama of $< p >$ agree well with zeros values of correlations between $z = 12r_e$ and $z = 25r_e$, i.e. between the 3rd and the 5th shock cells. It can be moreover noted that the correlations are positive when the flow is compressed, and negative when it is expanded.

The successive bands of correlations may thus be related to the shock-cell structure. The snapshot of fluctuating pressure presented in figure 1 displays upstream-propagating acoustic waves associated with the screech noise component. In the previous study performed by de Cacqueray *et al.*[10] for this jet, the screech fundamental frequency was found to be $St_{screech} = 0.08$. Therefore a time delay $\tau_{screech}$ based on the local shock-cell length L_{shock} and on the screech frequency $f_{screech}$ is built as:

$$\tau_{screech}(z) = \tau_0(z_0) + \int_z^{z_0} \frac{dz}{u_{screech}(z)}$$

where z_0 is a point chosen arbitrarily along the jet axis, τ_0 is the acoustic time delay between the point at z_0 and the acoustic probe, and $u_{screech} = f_{screech} L_{shock}$ is the convection velocity associated with the screech component. The screech time $\tau_{screech}$ is represented in figure 19(b) for $z_0 = 18.5r_e$. At this location, the local shock-cell length estimated from the figure 2(a) is $L_{shock} = 4.3r_e$. The trajectory provided by $\tau_{screech}$ is found to correspond to the direction of the bands of correlations, which suggests that these bands may be associated with the screech component. In screeching jets, Panda[26] has for instance observed shock motions along the jet axis at the screech frequency. This trend might explain the correlation bands presented in the figure 19(b).

V. Conclusion

In the present paper, the noise generation and propagation are investigated for an initially laminar and overexpanded jet at Mach number 3.3 and Reynolds number 10^5. The non-linear effects on the propagation of the acoustic waves are first clearly shown. They appear to be strong up to about 240 radii from the nozzle exit. The normalized cross-correlations between the flow quantities and the acoustic field in the downstream direction are then evaluated. A sound source is identified near the end of the potential core. It displays similarities with the sound source observed in subsonic jet, which can be attributed to the intermittent intrusion of vortical structures into the jet core.[11] Other sound sources are noticed over a wider region than the previous one. They may be connected to supersonic convection of turbulent vortices. Finally, bands of correlations have been observed between the 3rd and the 5th shock cells for density/acoustic correlations on the jet axis. They have been attributed to the shock motions at the screech tone frequency.

Acknowledgments

The work presented in this paper is sponsored by the CNES (Centre National d'Etudes Spatiales). The authors would like to thank the task monitor Hadrien Lambaré for his support. This work was granted access to the HPC resources of IDRIS under the allocation 2011-020204 made by GENCI (Grand Equipement National de Calcul Intensif).

References

[1] Tam, C., "Supersonic jet noise," *Annual Review of Fluid Mechanics*, Vol. 27, 1995, pp. 17-43.

[2] Laufer, J., Schlinker, R. and Kaplan, R.E., "Experiments on supersonic jet noise," *AIAA Journal*, Vol. 14, 1976, pp. 489-504.

[3] Veltin, J., Day, B.J., and Mclaughlin, D.K., "Correlation of flowfield and acoustic field measurements in high-speed jets," *AIAA J.*, Vol. 49, No. 1, 2011, pp. 150-163.

[4] Lele, S.K., "Compact finite difference schemes with spectral-like resolution," *Journal of Computational Physics*, Vol. 103, No. 1, 1992, pp. 16-42.

[5] Bogey, C. and Bailly, C., "A family of low dispersive and low dissipative explicit schemes for flow and noise computations," *Journal of Computational Physics*, Vol. 194, No. 1, 2004, pp. 194-214.

[6] Berland, J.,Bogey, C., Marsden, O. and Bailly, C., "High-order, low dispersive and low dissipative explicit schemes for multi-scale and boundary problems," *Journal of Computational Physics*, Vol. 224, No. 2, 2007, pp. 637-662.

[7] Freund J.B, Lele, S.K. and Moin, P., "Numerical simulation of a Mach 1.92 turbulent jet and its sound field," *AIAA Journal*, Vol. 38, No. 11, 2000, pp. 2023-2031.

[8] Bogey, C. and Bailly, C., "Computation of high Reynolds number jet and its radiated noise using large eddy simulation based on explicit filtering," *Computer and Fluids*, Vol. 35, No. 10, 2006, pp. 1344-1358.

[9] Berland, J., Bogey, C. and Bailly, C., "Numerical Study of screech generation in a planar supersonic jet," *Physics of Fluids*, Vol. 19, No. 7, 2007, pp. 1-14.

[10] de Cacqueray, N., Bogey, C. and Bailly, C., "Investigation of a high-Mach-number overexpanded jet using large-eddy simulation," *Accepted in AIAA Journal*, 2011.

[11] Bogey, C. and Bailly, C., "An analysis of the correlations between the turbulent flow and the sound pressure field of subsonic jets," *Journal of Fluid Mechanics*, Vol. 583, 2007, pp. 71-97.

[12] Bogey, C. and Bailly, C., "Influence of nozzle-exit boundary layer conditions on the flow and acoustic fields of initially laminar jets," *Journal Fluid Mechanics*, Vol. 663, 2010, pp. 507-538.

[13] Bogey, C., Marsden, O. and Bailly, C., "Large-eddy simulation of the flow and acoustic fields of a Reynolds number 10^5 subsonic jet with tripped exit boundary layers," *Physics of Fluids*, Vol. 23, 035105, 2011, pp. 1-20.

[14] Gee, K.L., Sparrow, V.W., James, M.M., Downing, J.M., Hobbs, C.M., Gabrielson, T.B., and Atchley, A.A., "The role of nonlinear effects in the propagation of noise from high-power aircraft," *J. Acoust. Soc. Am.*, Vol. 123, No. 6, 2008, pp. 4082-4093.

[15] Saxena, S., Morris, P.J. and Viswanathan, K., "Algorithm for the nonlinear propagation of broadband jet noise," *AIAA Journal*, Vol. 47, No. 1, 2009, pp. 186-194.

[16] Panda, J. and Seasholtz, R.G., "Experimental investigation of density fluctuations in high-speed jets and correlation with generated noise," *Journal of Fluid Mechanics*, Vol. 450, 2002, pp. 97-130.

[17] Panda, J., Seasholtz, R.G., Elam, K.A. "Investigation of noise sources in high-speed jets via correlation measurements," *Journal of Fluid Mechanics*, Vol. 537, 2005, pp. 349-385.

[18] Bogey, C., de Cacqueray, N. and Bailly, C., "A shock capturing methodology based on adaptative spatial filtering for high-order non-linear computations," *Journal of Computational Physics*, Vol. 228, No. 5, 2009, pp. 1447-1465.

[19]Mohseni, K. and Colonius, T., “Numerical treatment of polar coordonate singularities,” *Journal of Computational Physics*, Vol. 157, No. 2, 2000, pp. 787-795.

[20]Bogey, C., de Cacqueray, N. and Bailly, C., “Finite differences for coarse azimuthal discretization and for reduction of effective resolution near origin of cylindrical flow equations,” *Journal of Computational Physics*, Vol. 230, No. 3, 2011, pp. 1134-1146.

[21]Bogey, C. and Bailly, C. “Turbulence and energy budget in a self-preserving round jet: direct evaluation using large-eddy simulation,” *Journal of Fluid Mechanics*, Vol. 627, 2009, pp. 129-160.

[22]Bogey, C. and Bailly, C. “Three-dimensional non-reflective boundary conditions for acoustic simulations: far field formulation and validation test cases,” *Acta Acustica*, Vol. 8, No.4, 2002, pp. 463-471.

[23]Bogey, C., Barré, S., Juvé, D. and Bailly, C., “Simulation of a hot coaxial jet: direct noise prediction and flow-acoustics correlations,” *Physics of Fluids*, Vol. 21, 2009.

[24]Tam, C.K.W., Viswanathan, K., Ahuja, K.K. and Panda, J., “The sources of jet noise: experimental evidence,” *Journal of Fluid Mechanics*, Vol. 615, 2008, pp. 253-292.

[25]Ffowcs Williams J.E. and Maidanik, G., “The Mach wave field radiated by supersonic turbulent shear flows,” *Journal of Fluid Mechanics*, Vol. 21, 1965, pp. 641-657.

[26]Panda, J., “Shock oscillation in underexpanded screeching jets,” *Journal of Fluid Mechanics*, Vol. 363, 1998, pp. 173-198.